Supplementary

Emergent collective alignment gives competitive advantage to longer cells during range expansion

Nathan van den Berg[1†], Kristian Thijssen[1†], Thu Trang Nguyen[1†], Adrien Sarlet[1†], Mireia Cordero[1], Alba García Vázquez[1], Namiko Mitarai[1], Amin Doostmohammadi[1], and Liselotte Jauffred[1]

[1]The Niels Bohr Institute, University of Copenhagen, Blegdamsvej 17, DK-2100 Copenhagen O, Denmark
[†]These authors contributed equally
[1]Correspondence: mitarai@nbi.ku.dk, doostmohammadi@nbi.ku.dk, jauffred@nbi.ku.dk

MATERIALS AND METHODS

Bacterial strains

We used three subpopulations of the non-motile (1) *Escherichia coli* B strain REL606: the wild-type strain (WT) and the *mreB* mutants (2) REL606*mreB*^{A53S} (AS) and REL606*mreB*^{A53K} (AK) (3) (Table 1). The *mreB* gene in bacteria codes for the filament protein MreB, which is homologous to actin in eukaryotic cells (4). Depletion of the *mreBCD* operon in *E. coli* leads to spherical, enlarged, and eventually lysed cells (5). More specifically, MreB is responsible for maintaining the rod-like cell shape of *E. coli* cells by promoting cell wall growth in regions of negative cell wall curvature. Therefore, its depletion leads to homogeneous cell wall growth (6) by increasing the helical pitch of the filaments, causing shortening and widening of the bacteria's shape (7). All our strains carried a plasmid that constitutively expressed kanamycin resistance and either GFP, pmaxGFP (pmaxCloning-Vector, Lonza), with excitation/emission of 487/509 nm or RFP, pTurboRFP (pmaxCloning-Vector, Lonza), of 553/574 nm (8).

Name	Strain	Relevant characteristics	Reference
WT	REL606	Ancestral strain. Ara(−), StrepR	(9)
AS	REL606*mreB*^{A53S}	REL606 with *mreB*^{A53S} allele	(3)
AK	REL606*mreB*^{A53K}	REL606 with *mreB*^{A53K} allele	(3)

Table 1: *Escherichia coli* strains used in the study (kind gifts from the Kevin Foster Lab).

Culture media

Throughout this study, we alternated between the following two media: rich Lysogenic broth (LB) and M63 minimal media (M63+glu) supplemented with 30 µg/ml kanamycin sulphate (≥ 95%, K1377, Sigma-Aldrich) to retain fluorescence, unless otherwise stated. For agar plates, we used either 0.5% or 1.5% BD Bacto™ agar (10455513, Fisher Scientific).

M63+glu The 5X M63 salt solution was composed of 15 g/l anhydrous KH_2PO_4 (≥98.0%, P9791, Sigma-Aldrich), 35 g/l anhydrous K_2HPO_4 (≥99.0%, 60353, Sigma-Aldrich), 10 g/l $(NH_4)_2SO_4$ (≥99.0%, 09978, Sigma-Aldrich), 2.5 ml 20 mM $FeSO_4$ (≥99.5%, 44970, Sigma-Aldrich), 20 mM Na-Citrate (≥99.5%, 71402, Sigma-Aldrich). The M63 minimal media was composed of 20% 5X M63 salt, 1 µg/ml thiamine hydrochloride (≥99%, T4625, Sigma-Aldrich), 2 mM $MgSO_4$ (≥99.5%, 63138, Sigma-Aldrich), 2 mg/ml glucose (≥99.5%, G7528, Sigma-Aldrich), dissolved in Millipore water.

LB The Luria-Bertani (LB) medium was composed of 10 g/l Gibco™ Bacto™ tryptone (16279751, Fisher Scientific), 5 g/l Gibco™ Bacto™ yeast extract (16279781, Fisher Scientific) and 5 g/l NaCl (≥99%, S9888, Sigma-Aldrich) dissolved in Millipore water.

Cell culture

For starting the culture, bacteria from frozen glycerol stocks were streaked on LB or M63+glu agar (1.5%) plates to obtain microcolonies after overnight growth at 37 °C. A single colony from the streak plates was transferred into 2 ml LB and incubated overnight at 37 °C under constant shaking to prevent biofilm formation. The OD_{600} of the overnight cultures was measured after a 10-fold dilution (IMPLEN NanoPhotometer C40) to control the strain proportions in the resulting suspension.

Imaging

Confocal laser scanning microscopy (CLSM) On a Leica DMI6000 CS SP5 (Leica, Wetzlar, Germany) we used the Ar (488 nm) and HeNe (543 nm) laser lines sequentially to excite GFP (detection: 498 −536 nm) and RFP (detection: 568 −641 nm), respectively. We alternated between the following magnification objectives: 5× air objective (Nplan5×0.12PHO, Leica), 20× air objective (NplaL20x0.40NA, Leica), and 100× oil immersion objective (100×0.17/D/HCX/PL/APO, Leica).

Fluorescence microscopy We used a Nikon ECLIPSE Ti microscope (Nikon, Tokyo, Japan) paired with an Andor Neo camera (Andor, Belfast, UK). GFP and RFP were excited by a Hg lamp using the FITC (FITC Filter Cube Set, Olympus, York, UK) and Texas Red cubes (Texas Red^{TM} Filter Cube Set, Nikon, Tokyo, Japan), respectively. In combination with one of the following objectives: 4× air immersion objective (Nikon, Plan Fluor, 4x/0.13, ∞/1.2 WD 16.5), 20× air immersion objective (Nikon, Plan Fluor, 20x/0.50, ∞/0.17 WD 2.10) and 100× oil immersion objective (Nikon, Plan Apochromat λ, 100x/1.45 Oil, ∞/0.17 WD 0.13).

Growth rate measurements

Starting from overnight cultures (WT+GFP, WT+RFP, AS+GFP, AS+RFP, AK+GFP, AK+RFP) in M63+glu liquid medium, we diluted 100× in M63+glu to final volumes of 5 ml. The cultures were incubated at 37 °C and the OD_{600} was measured at regular intervals (1.25 h-1.75 h) for 5 −6 h, while making sure to dilute appropriately to stay within the optimal range of the spectrometer. In parallel, we collected samples for CFU measurements. We diluted the sample to adjust the CFU count to ∼100/plate, and 100 µl was plated on 3 LB agar (1.5%) plates and incubated overnight before CFU were counted.

Cell aspect ratio and volume measurements

Sample preparation and imaging We collected samples (WT+GFP, AS+GFP, AK+GFP) in the stationary phase (i.e. immediately following overnight culture) and the log phase (3 h after dilution) for imaging. Single droplets of bacterial cultures were deposited on cover slides (#1.5) and imaged using fluorescence microscopy and the 100× objective.

Image analysis We measured the length, l, and width, w, of cells using the line tool in Fiji ImageJ to calculate the aspect ratio, l/w, and corresponding volumes:

$$V_{cell} = \frac{4}{3}\pi\left(\frac{w}{2}\right)^3 + \pi\left(\frac{w}{2}\right)^2 (l - w)\,, \tag{1}$$

where cell shapes were approximated to be cylinders with hemispherical ends. Using Eq. 1, we found the volume ratio between the WT and AK strains in the stationary phase to be ∼ 1.3.

Cell density measurements

For each strain (WT+GFP, WT+RFP, AK+GFP, AK+RFP) we plated 100 µl of diluted overnight culture on LB plates with agar (1.5%), which were incubated overnight (37 °C), before CFU were counted. We found similar results for the two colours and measured the (combined) conversion at $OD_{600} = 1$ to be $1.6 \cdot 10^9$ CFU and $0.7 \cdot 10^9$ CFU, for WT and AK, respectively. Therefore, the cell number ratio between the WT and AK strains in stationary phase (same OD_{600}) was measured to be ∼ 2.2.

2D competition

Sample preparation and imaging Starting from overnight cultures, we adjusted the ratios (based on OD_{600}) of the longer cells (WT or AS) versus the shorter (AS or AK) to $\zeta \in \{1, 0.1, 0.01, 0.001\}$ and diluted to a final (and combined) OD_{600} of 0.3. The diluted cell culture was inoculated in 0.5 µl droplets on M63+glu plates with agar (1.5%). After either 20 h or 3 days of incubation (37 °C), we imaged the colonies using the CLSM and the 5× objective. A vertical range of 100 µm was scanned and the resulting 3D images had voxel sizes of $(x, y, z) = (6.07, 6.07, 10)$ µm.

Pre-processing In many cases, colonies had outgrown the field of view (3.1 mm × 3.1 mm), so we stitched 4 images together using the Pairwise Stitching plugin in Fiji ImageJ (10). We made a maximum intensity pixel projection of each stack to get a flattened (x, y)-image of pixel size $(x, y) = (6.07, 6.07)$ µm.

Intensity adjustment of colour channels To boost the contrast between the two channels, we divided channels (GFP and RFP) with each other to amplify the pixel value range of the two channels. Thus, for each pixel, we calculated a new intensity value, $p(x, y)'$, using a re-scaling value of 100 (8-bit image), such that:

$$p(x, y)' = \frac{p_{\mathrm{GFP}}(x, y) + 100}{p_{\mathrm{RFP}}(x, y) + 100}, \tag{2}$$

where p_{GFP} and p_{RFP} are the pixel values from the GFP and RFP channels, respectively. We found this method to be particularly useful in image areas with significant intensity variations (e.g., around the homeland) and for background removal (11).

Pixel classification For further analysis, we wanted all pixels to be classified as either GFP or RFP (never both). Therefore, we used the rescaled pixel intensities, $p(x, y)'$, distribution of the image and – consistently – found two peaks corresponding to GFP and RFP, and using Otsu's method, we estimated the threshold value to classify the pixels.

Competition strength as a function of the radial vector in 2D Colonies had clearly detectable regions and we defined the homeland as the well-mixed centre region, which roughly corresponded to where the original inoculation droplet was deposited. The boundary of this region was found by manual fitting of a circle and we identified the centre of this circle as the starting point of the radial vector $\mathbf{r}(t)'$, and the homeland boundary $\mathbf{r}(t = 0)$ (after which clear sectors first appear). To account for variations in drop size, we defined the translated radial distance as

$$r(t) = |\mathbf{r}(t)'| - |\mathbf{r}(t = 0)|. \tag{3}$$

We defined the ensemble-averaged strength of N colonies to be the re-scaled occupancy of the GFP-expressing (and longer) bacteria at a given radial length $r(t)$ as the sum over the following fraction:

$$\mathcal{S}(r) = \frac{2}{N} \sum_{n=1}^{N} \frac{C^{(n)}_{\mathrm{GFP}}(r(t))}{C^{(n)}(r(t))} - 1, \tag{4}$$

where $C^{(n)}(r(t))$ is the total number of pixels of the circle of the n-th colony at radial distance $r(t)$ and $C^{(n)}_{\mathrm{GFP}}(r(t))$ is the number of pixels occupied by GFP-expressing bacteria, such that $C^{(n)}(r(t)) = C^{(n)}_{\mathrm{GFP}}(r(t)) + C^{(n)}_{\mathrm{RFP}}(r(t))$. Defined like this, $\mathcal{S}$ had the value of 1 (-1) when the GFP-expressing (RFP-expressing) cells had taken over the complete perimeter at a specific radial distance. To compare the $\mathcal{S}$ at a specific time, we defined $t_1 = 1.5$ days as halfway from the homeland border to the front of a colony after 3 days of incubation.

Competition in isogenic bacteria Starting from overnight cultures, we inoculated 1:1 ($\zeta = 1$) two subpopulations (expressing GFP or RFP) of the same strain (WT/WT, AS/AS, or AK/AK) with the same fitness and shape at $\mathrm{OD}_{600} = 0.3$. Plates were incubated for 20 h and CLSM imaged. We found patterns of spatially segregated lineages with a constant number of sectors (Supplementary Fig. S11); well in accordance with earlier findings (8, 12).

Zoom in on 2D competition isogenic boundaries Plates were incubated (37 °C) for 3 days, before cutting out the colony and the according square of agar and placing it upside down in a glass-bottomed culture well (HBST-5040, WillCo Wells B.V.). The colonies were imaged with sequential z-stacks using CLSM in combination with the 100× objective and the resulting voxel size in $(x, y, z) = (0.30, 0.30, 0.99)$ µm.

Varying seeding density We repeated the competition experiment (20 h) for WT/AK but for serial dilutions of seeding density. The co-culture of WT and AK mixed 1:1 and $\mathrm{OD}_{600} = 0.3$ was diluted 10-, 100-, and 1000-fold. We found the mixing of genotypes reduced in the homeland (i.e., patch sizes enlarged), but WT was still able to completely dominate the expansion front (Supplementary Fig. S3). So even though the seeding density regulates patch sizes (13, 14), the longer cell still wins.

Single-cell resolution time-lapses

Sample preparation One colony of each WT and AK was transferred separately into 3 ml LB medium and incubated overnight (37 °C) under constant shaking. The OD_{600} of the overnight cultures were measured and they were mixed in equal proportions ($\zeta = 1$), before 10-fold dilution and inoculation on M63+glu agar (1.5%) plates. Shortly following the inoculation, a rectangular piece of agar was cut out, flipped, and transferred upside down into glass-bottomed culture well (HBST-5040, WillCo Wells B.V.) and sealed with Parafilm®.

Single-cell resolution time-lapses The colonies were imaged in our inverted fluorescence microscope using the 100× objective. Fluorescence images were acquired with a frame rate of 2/h during 12 h. In addition, z-stacks were collected over a total range of 2 µm (0.5 µm spacing) for each time frame to cope with the relative roughness of the agar substrate surface at high magnification.

Data analysis The z-stacks were high-pass filtered and summed into a single image using a custom-made MATLAB procedure, thereby collapsing all the sharpest regions into a single plane. Bacteria were segmented by thresholding each time frame multiple times (twice for AK, thrice for WT) to consider variations in intensity and saturation within a single time frame. The binary images resulting from different thresholds (of the same time frame) were summed to collect as many bacteria as possible, despite non-uniform contrasts. Bacteria were detected using the Regionprops function in MATLAB (Image Processing Toolbox version 11.7). The function returned the (x,y)-coordinates and the orientation of each bacterium (major axis of the ellipse that has the same second-moments as the bacterium pixels region).

The local nematic order parameter q for a bacteria n, is calculated by locating the $N_n = 8$ nearest neighbours n_i of the same strain and then using the definition:

$$q_n = \frac{1}{N_n} \sum_{n_i}^{N_n} \left(\frac{3}{2} \cos^2 \theta_i - \frac{1}{2}\right) \tag{5}$$

with θ_i the orientation of the neighbouring bacteria orientation.

3D competition

Encapsulating bacteria in inoculation beads We produced four batches of 2.5% agarose inoculation beads containing different ratios of WT+GFP and AK+RFP following the procedure outlined in Ref. (15), excepting the following modifications: i) Cell densities in the beads were either $OD_{600} = 0.65$ or $OD_{600} = 1.45$ ($OD_{600} = 4$ or $OD_{600} = 8.6$ in the cell mix) for $1/\zeta_n \in \{0.25, 12, 16\}$ and $1/\zeta_n = 47$, respectively. The latter was obtained by up-concentration through centrifugation of the overnight cultures. Varying the densities ensured reasonable numbers of (WT+GFP), despite low ratios (high $1/\zeta_n$). We ii) filtered the PBS-bead suspensions through strainers with mesh sizes of 70 , 50 , and 40 µm and let at least 10 ml additional PBS flow through the strainers to wash off the remaining silicone oil. We collected the beads in the 40 µm strainer (diameters of 40 −50 µm) by turning it upside down and flushing with 6 −9 ml LB. More details can be found in the associated protocol (16).

Mono-strain 3D colonies As a control, we also prepared beads with two colours of the same strain. We followed the exact same procedure but with a different bacteria mixture: Overnight cultures were mixed 1:1 by adjusting the OD_{600} (WT+GFP/WT+RFP, AK+GFP/AK+RFP, AS+GFP/AS+RFP) and diluted in LB to a final (overall) $OD_{600} = 0.07$ (0.4. in the cell mix).

Bead concentration measurements To measure the strain ratios and number of cells within the inoculation beads, we did serial dilutions ($10^{-7} - 10^{-5}$) of the spare cell mixture from the encapsulation process. We plated 100 µl of the dilution on LB agar (1.5%) plates and incubated overnight. From the number and colour of CFU, we deduced i) the ratio of WT to AK cells ($1/\zeta_n$) and ii) the overall cell concentration of the mixture. Based on these results, we estimated the number of cells encapsulated within a bead by modelling the beads as perfect spheres with a radius of 45 µm. The strain ratios were estimated from counting 1606, 2900, 3918, and 3472 CFU for $1/\zeta_n \in \{0.25, 12, 16, 47\}$, respectively.

As the small size limited the number of cells per bead and as the strains had different cell volumes (Table 1 in the main text), we defined a strain ratio, ζ_n, as the ratio of CFU of the longer strain versus the shorter (measured before encapsulation in the beads). We found $1/\zeta_n \in \{0.25, 12, 16\}$ with $OD_{600} = 0.65$ and $1/\zeta_n = 47$ with $OD_{600} = 1.45$; the higher density for the latter ensured WT cells in most beads at this extreme ratio.

Embedment of inoculation beads in 0.5% agar To investigate competition in 3D, we embedded the inoculation beads within a 0.5% agar growth medium. We followed the protocol outlined in (15), excepting the following adaptions: i) Frozen bead stocks were diluted with LB (based on the measured concentration of beads per 1 ml frozen stock) aiming for 10 beads per well. Specifically, we diluted $\{650, 970, 130, 85\}$ µl of frozen bead stock in 1 ml LB for $1/\zeta_n \in \{0.25, 12, 16, 47\}$, respectively. We counted on average 10.9±3.3 beads per well and ii) we incubated all colonies for 10 h.

3D colony imaging After incubation, wells were preserved at 4 °C until imaging (< 24 h) using the CLSM and the 20× objective (discarding colonies that had reached the agar-glass or the agar-air interface). For bi-coloured colonies, we recorded two sequential (RFP then GFP) z-stacks with a resulting voxel volume of $(x, y, z) = (1.51, 1.51, 1.33)$ µm. For each strain ratio $(1/\zeta_n)$, we collected images from 4-5 different wells (> 40 colonies in total). As a control, we also mixed 1:1 (i.e., $\zeta_n = 1$) two subpopulations (expressing GFP or RFP) of the same strains and found that surface coverage was similar for both strains (Supplementary Fig. S12). In the case of WT/WT, this is well in accordance with earlier findings (15).

Segmentation of 3D images The 3D colony images were processed, segmented, and filtered for the surface using BiofilmQ (17) and Fiji/Image J (18). Only colonies expressing both strains were segmented, following the exact process described in Ref. (15).

Competition strength as a function of time in 3D We defined the ensemble-averaged strength of GFP-expressing bacteria (WT) on the colony surface as the re-scaled sum over the area fraction:

$$\mathcal{S}_3(t) = \frac{2}{N}\sum_{n=1}^{N}\frac{A^{(n)}_{\mathrm{GFP}}(t)}{A^{(n)}(t)} - 1, \tag{6}$$

where $A^{(n)}_{\mathrm{GFP}}(t)$ is the area of GFP-expressing bacteria and $A^{(n)}(t)$ is the total surface area of the n-th colony at time t, such that $A^{(n)}(t) = A^{(n)}_{\mathrm{GFP}}(t) + A^{(n)}_{\mathrm{RFP}}(t)$. In contrast to the 2D case, $\mathcal{S}_3$ is a function of t (instead of $r(t)$) as it refers to the surface at a given t, with varying $r(t)$. For colonies whose visible surface only expressed one of the two strains, we assigned $A^{(n)}_{GFP} = 1$ (GFP-mono-coloured) or $A^{(n)}_{GFP} = 0$ (RFP-mono-coloured). We also calculated the expectation value of the subset of N originating from pure RFP-expressing cells from estimated number of cells per bead (CFU/V_{bead}), the total number of colonies (N), and the WT/AK ratio (ζ_n); assuming a binomial distribution.

Statistics All mean values are given as mean plus/minus the standard deviation (SD) or the standard error of the mean (SEM), when this is stated and only when data are tested against the null hypothesis that it is normally distributed. The normal distributions of $\mathcal{S}$ were assessed with Shapiro-Wilk tests. Their distributions were compared between the WT and AK strains with Mann-Whitney U Tests. The significance of the differences in ν were evaluated with a Students t-test.

Computational models

Particle model The particle-based model is based on the work presented and described in (19). A single bacteria is described as a rod, α, consisting of a rigid chain of a number of Yukawa segments, n_α, separated by length, l_α, with segments of different rods repelling one another with a Coulomb-like point potential with potential strength, $U_0 = 250$ (previous work has shown that results are independent on U_0 provided it is large enough (20)), resulting in a total potential, U. The Yukawa screening length, λ, is taken as the width of the particle with the aspect ratio of the rod: $L = n_\alpha l_\alpha/\lambda$.

Every time step, Δt, the length of bacteria α increases with $\delta L = \gamma \delta t \mathbf{randn}$ with **randn** a random number between 0 and 1 with uniform distribution and the growth rate, γ. The number of segments and n_α and spacing l_α is then redefined, such that n_α is always greater than two and $l_\alpha < \lambda$. After the rod has reached the division length l, the particle is split into two. Simulations are normalised by the average time for a single particle to go from its smallest size to the division aspect ratio l.

The equations of motion that describe the translation and rotation of each rod α are (19)

$$f_t \frac{\partial \vec{r}_\alpha}{\partial t} = -\frac{\partial U}{\partial \vec{r}_\alpha} \tag{7}$$

$$f_r \frac{\partial \theta_\alpha}{\partial t} = -\frac{\partial U}{\partial \theta_\alpha}, \tag{8}$$

where $\vec{r}_\alpha$ and θ_α are the centre and orientation of rod α, respectively.

At time zero, 40 rods are initialised in a small area with ten rods having division aspect ratio, l_L, and random aspect ratios (uniform distribution) between $l_L/2$ and l_L and thirty rods having division aspect ratio, l_S, and random aspect (uniform distribution) ratios between $l_S/2$ and l_S, such that $\zeta = 0.25$.

Competition strength in the particle model To determine the competition strength $\mathcal{S}_f(t)$ at the interface at it evolves over time, we count all particles that exist in the front. We do this by dividing the colony into 10 slices (with centre at the centre of mass of the colony), determine the particle that is furthest from the centre of the colony and then take into account all particles that inhabit up to 5 decay lengths λ into the colony.

The takeover rate, ν_{sim}, in the simulations is calculated from the $\mathcal{S}_f(t)$ curve of 10 different trajectories. The ν_{sim} is the linear fit from generation time 5.5 to time 7.5.

Continuum model To describe the bacterial colony on a course-grained level, we study the evolution of the nematic order parameter $\mathbf{Q} = 2q(\hat{n}\hat{n} - \frac{\mathbf{I}}{2})$, where q and $\hat{n}$ show the magnitude and orientation of the order, respectively, and $\mathbf{I}$ represents the identity tensor (21).

In line with other dry active nematic studies (22), (23), we use the dynamics of the $\mathbf{Q}$-tensor is described by the Beris-Edwards equation

$$\frac{DQ_{ij}}{Dt} = \chi E_{ij} + \Gamma H_{ij}, \tag{9}$$

with respect to a symmetric gradients E_{ij} (shear tensor) and anti-symmetric ω_{ij} (vorticity tensor) of a velocity field $\vec{u}$. We use the convected co-rotational time derivative $DQ_{ij}/Dt = (\partial_t + u_k\partial_k)\, Q_{ij} - \omega_{ik}Q_{kj} + Q_{ik}\omega_{kj}$.

In Eq. 9, χ is the aligning parameter (taken as 0.8) and $\Gamma = 0.1$ is the rotational diffusivity which along with H_{ij}, the molecular field, describes the relaxation of the $\mathbf{Q}$-tensor towards the minimum of a free energy described by:

$$\mathcal{F} = \frac{A}{2}(\mathbf{Q} : \mathbf{Q})^2 + \frac{K}{2}|\nabla \mathbf{Q}|^2. \tag{10}$$

The free energy includes the nematic alignment term (with coefficient $A = 0.01$) and an elastic term K which penalises gradients in the $\mathbf{Q}$ tensor.

Velocity is taken in the overdamped limit

$$f u_i = -\zeta\, \partial_j Q_{ij} + \eta \nabla^2 (\partial_j Q_{ij}) \tag{11}$$

where ζ is the activity coefficient related to a force dipoles generated from division events (positive to correspond to the extensile limit), which is balanced by frictional dissipation into the surface f and a small viscous dissipation with viscosity $\eta = 0.01$. The outer edge of the colony is taken by assuming high friction $f = 400$ outside a radius $R_{con} > 30$, while lower friction $f = 4$ is used inside the radius $R_{con} < 30$ (Supplementary Fig. S7). In addition, the incompressibility constraint is imposed on the total velocity field.

To distinguish the two bacterial concentrations, we introduce a phase-field binary order parameter ϕ, which evolves according to a Cahn-Hillard model

$$\partial_t \phi + \nabla \cdot (\vec{u}\phi) = \Gamma_\phi \nabla^2 \mu, \tag{12}$$

where $\mu = \frac{\delta \mathcal{F}}{\delta \phi} - \nabla \cdot \left(\frac{\delta \mathcal{F}}{\delta \nabla \phi} \right)$ is the chemical potential with $\Gamma_\phi = 0.3$ a mobility coefficient. We add to the free energy $\mathcal{F}$ a single well potential $f_{\text{DW}} = \frac{A_\phi}{2}\phi^2$ and an interfacial term $f_{\text{I}} = \frac{K_\phi}{2}(\nabla\phi)^2$ with $A_\phi = 0.002$ and $K_\phi = 0.02$ such that all bacterial phase-separation comes from activity dependence. We take $\phi < 0$ as the shorter bacteria and $\phi > 0$ as the longer bacteria. This is imposed by taking the phenomenological parameters ζ and K to be dependent on the local ϕ as:

$$\zeta = \begin{cases} 0.2 & \phi > 0 \\ 0.1 & \phi < 0 \end{cases} \tag{13}$$

$$K = \begin{cases} 0.09 & \phi > 0 \\ 0.05 & \phi < 0 \end{cases} \tag{14}$$

since it is well established that both orientational elasticity K and extensile activity due to division ζ are higher for higher aspect ratios (24, 25). All equations are solved using a finite-difference method and we initialise our system by taking $\phi = 0.01$ for radius $R < 25$, between $R = 25$ and $R = 30$ $\phi = -0.01$ and $\phi = 0$ for $R > 30$ in a system of size 80 by 80.

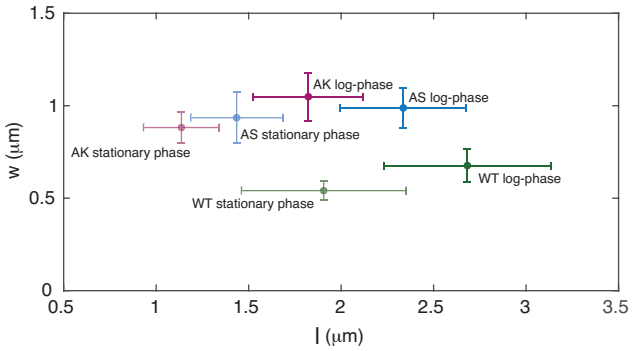

Figure S1. Aspect ratios for all strains used in this study. Width, w, versus length, l, of WT in both stationary phase (N = 32) and log-phase (N = 39), AS in both stationary phase (N = 47) and log-phase (N = 38), and AK in both stationary phase (N = 25) and log-phase (N = 33). Here stationary phase is measured directly in the overnight culture (0 h) and the log-phase 3 h after dilution (Fig. S2). The error bars are ±SD

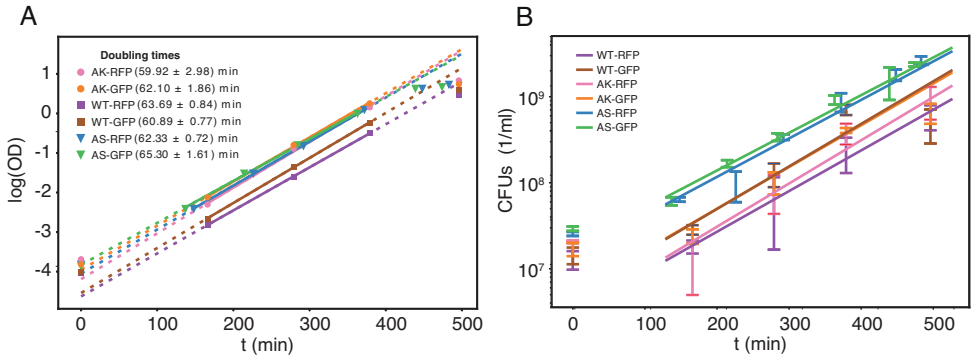

Figure S2. **A:** Growth rates for all strains used in this study. The optical density, OD_{600}, versus time, t, on a semi-logarithmic scale. The solid lines are linear fits to the data and the legends are the corresponding doubling times ±SD. **B:** Cell counts for WT (N = 3), AS, (N = 4), and AK (N = 3) strains used in this study. Colony-forming units (CFU) versus time, t, see legends. The solid lines are the growth rates from (A) for comparison and the error bars are ±SD.

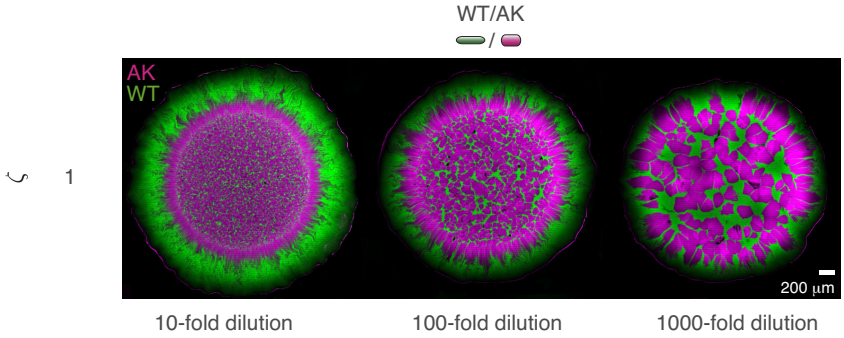

Figure S3. Seeding density regulates patch sizes but still the longer cell wins. Competition experiment (20 h) for serial dilutions of the optical density, OD_{600}, in a co-culture of WT and AK mixed 1:1 and diluted **A:** OD_{600}/10, **B:** OD_{600}/100, and **C:** OD_{600}/1000. For the latter, small channels of WT (green) are detectable between the patches of AK (magenta).

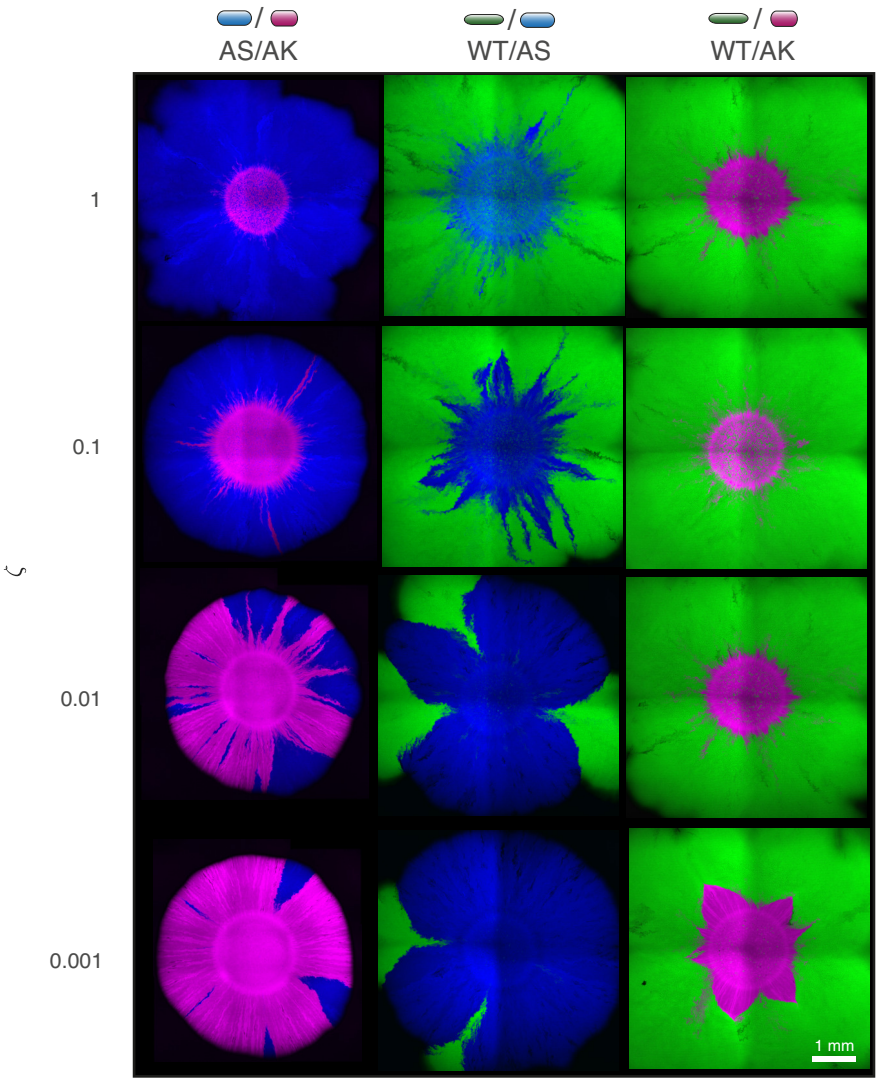

Figure S4. 3 days competition experiments. Example colonies (maximum intensity) z-projection from all strain combinations (AS/AK, WT/AS, WT/AK) imaged by CLSM. The scale bar corresponds to 1 mm. For WT/AK, with $\zeta = 0.001$, we only found 14 sectors surviving for 1.5 days (halfway from homeland to front) in 5 colonies, which closed off (i.e., sector was lost) rapidly hereafter. We note that even when the longer bacteria did not overtake the shorter within the explored time window, the sectors with longer bacteria tended to spread azimuthally with increasing r, indicating that they might eventually find their way to the expanding front.

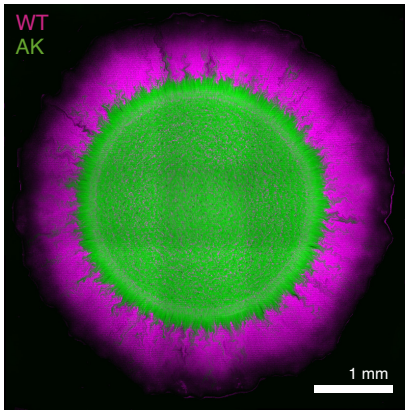

Figure S5. 20 h competition experiment with inverse colours. Example colonies (maximum intensity) z-projection from 1:1 ($\zeta = 0.1$) WT/AK combination imaged by CLSM. The scale bar corresponds to 1 mm.

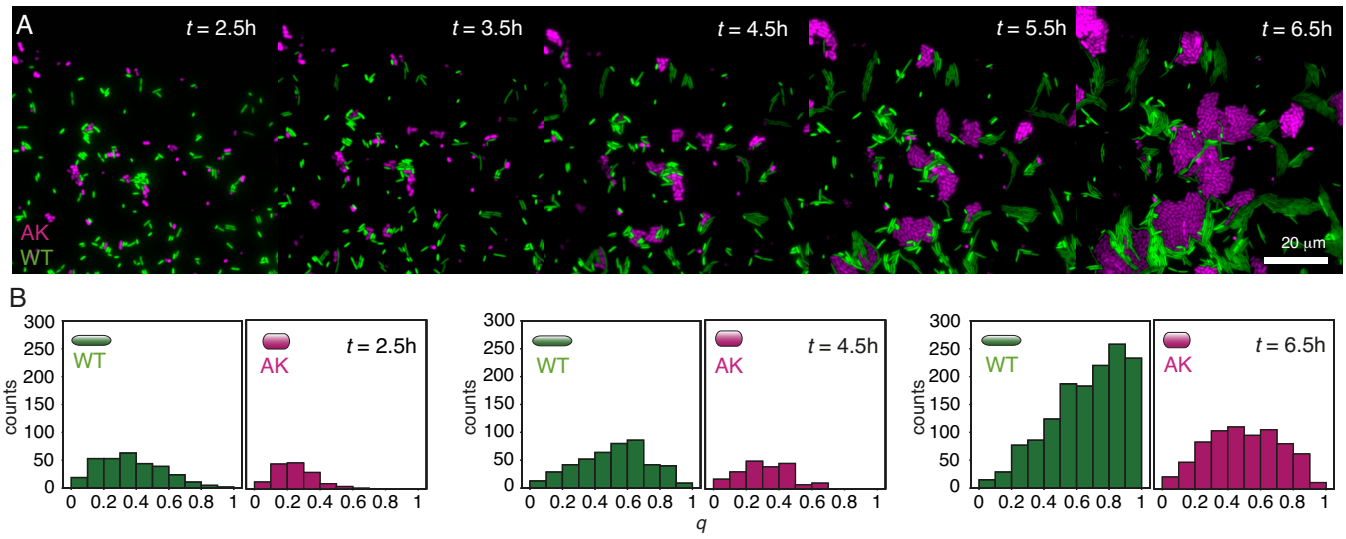

Figure S6. Long bacteria align more within clusters. **A:** Single cell (pseudo-coloured) time-lapses of competition between the two-colour wild-type (WT) and the *mreB* mutant (AK) at time points, t. Representative region of the larger images from which the data plotted in B was computed. The scale bar is 20 μm. **B:** The nematic order parameter, q, for WT and AK individually corresponding to every second time frame in (A) $t \in \{2.5, 4.5, 6.5\}$h.

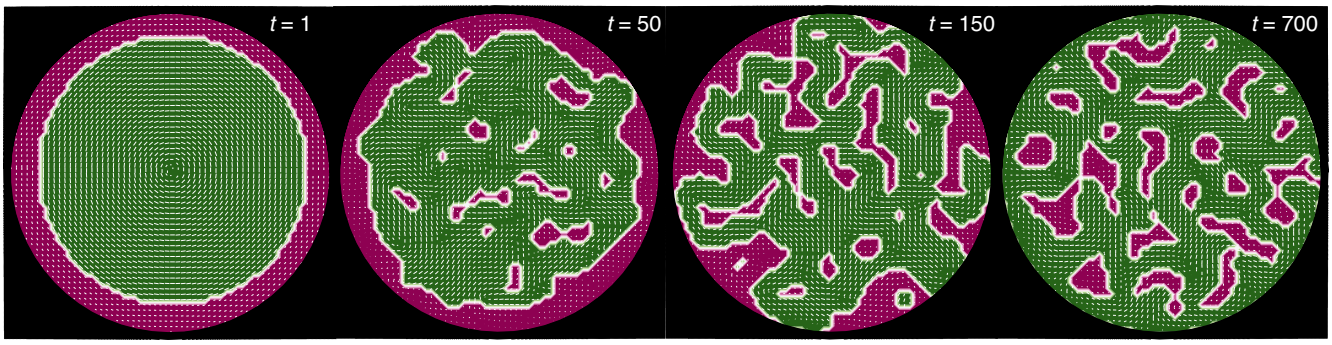

Figure S7. Time series of continuum dynamics where the phase representing short bacteria (magenta) starts at the edge while with time, the phase representing long bacteria (green) overtakes the short bacteria by forming pathways to the colony front.

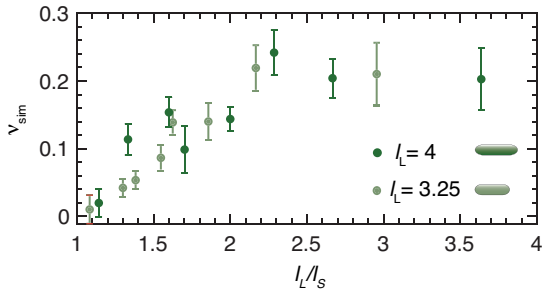

Figure S8. The takeover rate, μ_{sim}, (slope between $t = 30$ gen. to $t = 45$ gen.) for varying length ratios, l_L/l_S bacteria ratios, where long bacteria still have $w/l = 4$.

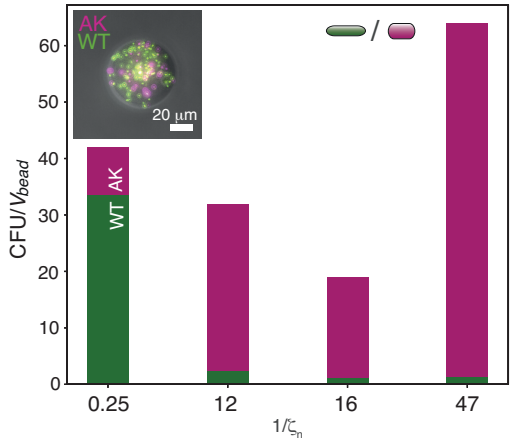

Figure S9. Cell concentrations in the various bead batches. The ratio of colony-forming units, CFU, versus the average bead volume, V_{bead}, for each strain ratio, $1/\zeta_n$. The colours indicate the fraction of WT (green) and AK (magenta). Inset: Merged image of the bright-field (grey), WT (green), and AK (magenta) of a bead with $1/\zeta_n = 0.25$. The scale bar corresponds to 20 µm.

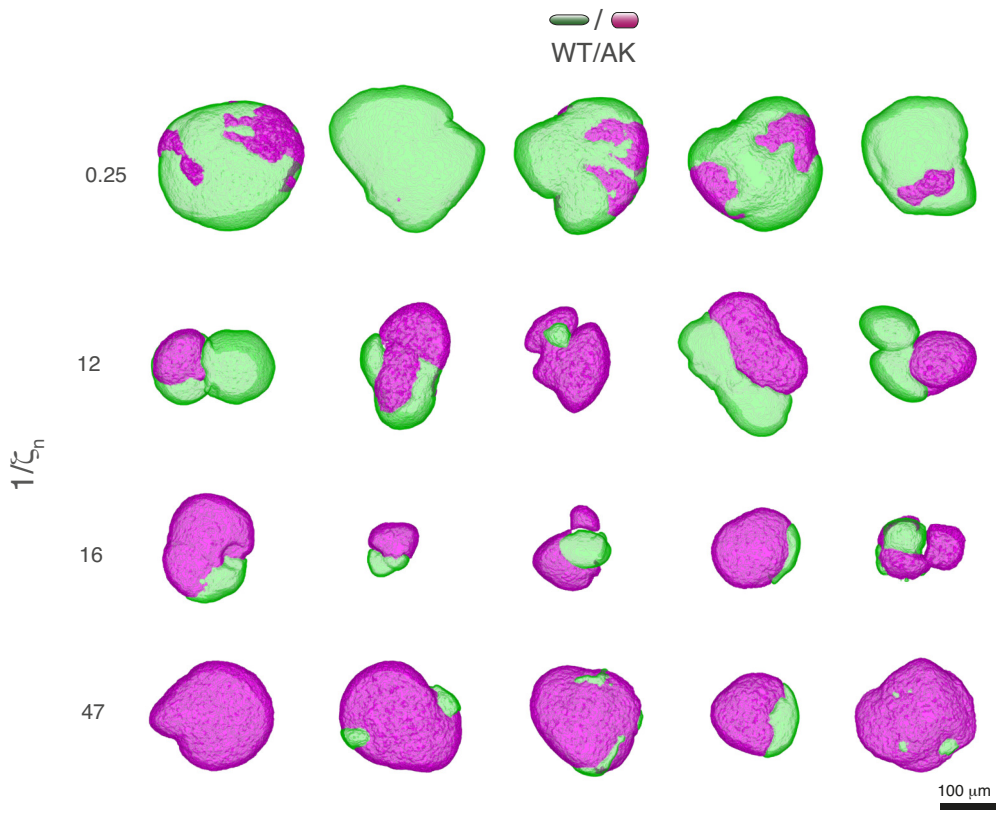

Figure S10. 10 h competition experiments. Example segmented masks of surfaces of two-coloured WT/AK colonies from all strain ratios imaged by CLSM. The scale bar corresponds to 100 µm.

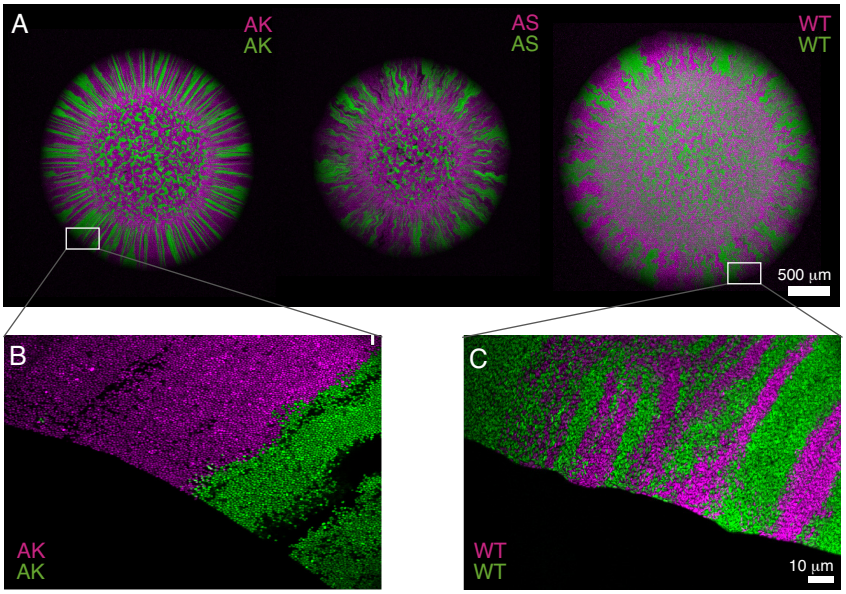

Figure S11. Segmentation patterns varies with genotype. **A:** The (maximum intensity) z-projections of example colonies (WT/WT, AS/AS, and AK/AK) imaged by CLSM after incubation (20 h). The scale bar corresponds to 500 μm. In the outer bands (i.e., outside of the homeland) the number of sectors are constant. Despite the general features, qualitative differences among the strains are clear: WT's sector boundaries are coarse (highly diffusive) and the mutants have straighter (less diffusive) boundaries. **B-C:** Single layer (pseudo-coloured) images of competition between the two-colours at the front of the colony: The *mreB* mutant (AK/AK) in (B) and wild-type (WT/WT) in (C). The scale bar is 10 μm.

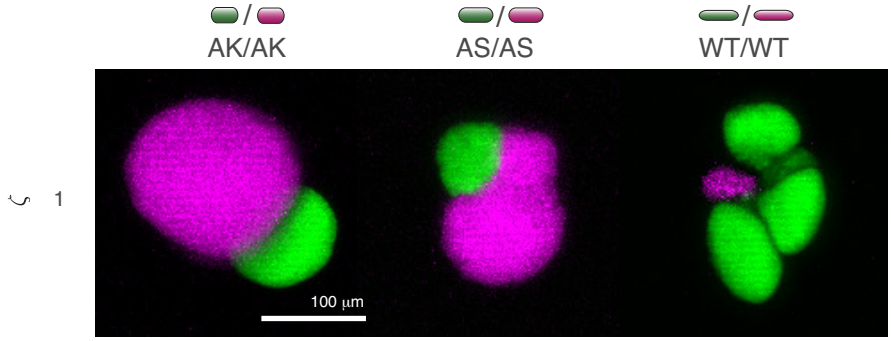

Figure S12. 10 h competition experiments. Example colonies (maximum intensity) z-projection from two-coloured strains colonies from all same strain ratios imaged by CLSM. The scale bar corresponds to 100 µm.

MOVIE LEGENDS

Movie 1

Long bacteria align over time with their neighbours and the expanding front. Time-lapse snapshots from (pseudo-coloured) fluorescence competition experiments between WT (green) and the *mreB* mutant AK (magenta), every 30 min, starting 1.5 h after inoculation.

Movie 2

Another example of how long bacteria align over time with their neighbours and the expanding front. Time-lapse snapshots from (pseudo-coloured) fluorescence competition experiments between WT (green) and the *mreB* mutant AK (magenta), every 30 min, starting 1.5 h after inoculation.

Movie 3

360°rotation view of a segmented mask of a 3D WT/AK colony surface. This mask is extracted from the first ($1/\zeta_n = 0.25$) image in Figure 4B. The scale bar corresponds to 100 µm.

REFERENCES

1. Studier, F. W., P. Daegelen, R. E. Lenski, S. Maslov, and J. F. Kim, 2009. Understanding the Differences between Genome Sequences of Escherichia coli B Strains REL606 and BL21(DE3) and Comparison of the E. coli B and K-12 Genomes. Journal of Molecular Biology 394:653–680. https://linkinghub.elsevier.com/retrieve/pii/S0022283609011383.

2. Wachi, M., and M. Matsuhashi, 1989. Negative control of cell division by mreB, a gene that functions in determining the rod shape of Escherichia coli cells. Journal of Bacteriology 171:3123–3127. https://journals.asm.org/doi/10.1128/jb.171.6.3123-3127.1989.

3. Monds, R. D., T. K. Lee, A. Colavin, T. Ursell, S. Quan, T. F. Cooper, and K. C. Huang, 2014. Systematic Perturbation of Cytoskeletal Function Reveals a Linear Scaling Relationship between Cell Geometry and Fitness. Cell Reports 9:1528–1537. https://doi.org/10.1016/j.celrep.2014.10.040.

4. Erickson, H. P., 2001. Evolution in bacteria. Nature 413:30–30. https://www.nature.com/articles/35092655.

5. Kruse, T., J. Bork-Jensen, and K. Gerdes, 2005. The morphogenetic MreBCD proteins of Escherichia coli form an essential membrane-bound complex. Molecular Microbiology 55:78–89. https://onlinelibrary.wiley.com/doi/10.1111/j.1365-2958.2004.04367.x.

6. Ursell, T. S., J. Nguyen, R. D. Monds, A. Colavin, G. Billings, N. Ouzounov, Z. Gitai, J. W. Shaevitz, and K. C. Huang, 2014. Rod-like bacterial shape is maintained by feedback between cell curvature and cytoskeletal localization. Proceedings of the National Academy of Sciences 111:E1025–E1034. https://pnas.org/doi/full/10.1073/pnas.1317174111.

7. Ouzounov, N., J. P. Nguyen, B. P. Bratton, D. Jacobowitz, Z. Gitai, and J. W. Shaevitz, 2016. MreB Orientation Correlates with Cell Diameter in Escherichia coli. Biophysical Journal 111:1035–1043. https://linkinghub.elsevier.com/retrieve/pii/S000634951630580X.

8. Smith, W. P. J., Y. Davit, J. M. Osborne, W. D. Kim, K. R. Foster, and J. M. Pitt-Francis, 2017. Cell morphology drives spatial patterning in microbial communities. Proceedings of the National Academy of Sciences 114:E280–E286. http://www.pnas.org/lookup/doi/10.1073/pnas.1613007114https://doi.org/10.1073/pnas.1613007114.

9. Lenski, R. E., M. R. Rose, S. C. Simpson, and S. C. Tadler, 1991. Long-Term Experimental Evolution in Escherichia coli. I. Adaptation and Divergence During 2,000 Generations. The American Naturalist 138:1315–1341. https://www.jstor.org/stable/2462549.

10. Preibisch, S., S. Saalfeld, and P. Tomancak, 2009. Globally optimal stitching of tiled 3D microscopic image acquisitions. Bioinformatics 25:1463–1465. https://academic.oup.com/bioinformatics/article/25/11/1463/332497.

11. van den Berg, N., 2023. Experimental study of bacterial cell shape's role in competition: elongated cells win in expanding mixed communities. Ph.D. thesis, University of Copenhagen, Copenhagen. https://nbi.ku.dk/english/theses/masters-theses/nathanael-van-den-berg/Nath_na_l_van_den_Berg.pdf.

12. Hallatschek, O., P. Hersen, S. Ramanathan, and D. R. Nelson, 2007. Genetic drift at expanding frontiers promotes gene segregation. Proceedings of the National Academy of Sciences 104:19926–19930. https://pnas.org/doi/full/10.1073/pnas.0710150104.

13. Eigentler, L., M. Kalamara, G. Ball, C. E. MacPhee, N. R. Stanley-Wall, and F. A. Davidson, 2022. Founder cell configuration drives competitive outcome within colony biofilms. The ISME Journal 16:1512–1522. https://www.nature.com/articles/s41396-022-01198-8.

14. van Gestel, J., F. J. Weissing, O. P. Kuipers, and Ã. T. Kovács, 2014. Density of founder cells affects spatial pattern formation and cooperation in Bacillus subtilis biofilms. The ISME Journal 8:2069–2079. https://www.nature.com/articles/ismej201452.

15. Vázquez, A. G., N. Mitarai, and L. Jauffred, 2024. Genetic mixing and demixing on expanding spherical frontiers. ISME Communications https://academic.oup.com/ismecommun/advance-article/doi/10.1093/ismeco/ycae009/7585292.

16. García Vázquez, A., T. T. Nguyen, N. Mitarai, and L. Jauffred, 2024. Cell encapsulation in inoculation beads for 3D growth experiments. ProtocolExchange https://protocolexchange.researchsquare.com/article/pex-2531/v1.

17. Hartmann, R., H. Jeckel, E. Jelli, P. K. Singh, S. Vaidya, M. Bayer, D. K. H. Rode, L. Vidakovic, F. Díaz-Pascual, J. C. N. Fong, A. Dragoš, O. Lamprecht, J. G. Thöming, N. Netter, S. Häussler, C. D. Nadell, V. Sourjik, Ã. T. Kovács, F. H. Yildiz, and K. Drescher, 2021. Quantitative image analysis of microbial communities with BiofilmQ. Nature Microbiology 6:151–156. https://www.nature.com/articles/s41564-020-00817-4.

18. Schindelin, J., I. Arganda-Carreras, E. Frise, V. Kaynig, M. Longair, T. Pietzsch, S. Preibisch, C. Rueden, S. Saalfeld, B. Schmid, J.-Y. Tinevez, D. J. White, V. Hartenstein, K. Eliceiri, P. Tomancak, and A. Cardona, 2012. Fiji: an open-source platform for biological-image analysis. Nature Methods 9:676–682. https://www.nature.com/articles/nmeth.2019.

19. Meacock, O. J., A. Doostmohammadi, K. R. Foster, J. M. Yeomans, and W. M. Durham, 2021. Bacteria solve the problem of crowding by moving slowly. Nature Physics 17:205–210. http://dx.doi.org/10.1038/s41567-020-01070-6https://www.nature.com/articles/s41567-020-01070-6.

20. Hamilton, W., 1971. Geometry for the selfish herd. Journal of Theoretical Biology 31:295–311. https://linkinghub.elsevier.com/retrieve/pii/0022519371901895.

21. De Gennes, P.-G., and J. Prost, 1993. The physics of liquid crystals. 83. Oxford university press.

22. Oza, A. U., and J. Dunkel, 2016. Antipolar ordering of topological defects in active liquid crystals. New Journal of Physics 18:093006. https://iopscience.iop.org/article/10.1088/1367-2630/18/9/093006.

23. Dell'Arciprete, D., M. L. Blow, A. T. Brown, F. D. C. Farrell, J. S. Lintuvuori, A. F. McVey, D. Marenduzzo, and W. C. K. Poon, 2018. A growing bacterial colony in two dimensions as an active nematic. Nature Communications 9:4190. http://dx.doi.org/10.1038/s41467-018-06370-3https://www.nature.com/articles/s41467-018-06370-3.

24. Kröger, M., and P. Ilg, 2007. Derivation of Frank-Ericksen elastic coefficients for polydomain nematics from mean-field molecular theory for anisotropic particles. The Journal of Chemical Physics 127. https://pubs.aip.org/jcp/article/127/3/034903/904677/Derivation-of-Frank-Ericksen-elastic-coefficients.

25. Wittmann, R., G. H. P. Nguyen, H. Löwen, F. J. Schwarzendahl, and A. Sengupta, 2023. Collective mechano-response dynamically tunes cell-size distributions in growing bacterial colonies. Communications Physics 6:331. https://www.nature.com/articles/s42005-023-01449-w.